THE ASTROPHYSICAL JOURNAL, 422:810–822, 1994 February 20

THE WOLF-RAYET BINARY V444 CYGNI UNDER THE SPECTROSCOPIC MICROSCOPE. I. IMPROVED CHARACTERISTICS OF THE COMPONENTS AND THEIR INTERACTION SEEN IN He I

SERGEY V. MARCHENKO,[1,2] ANTHONY F. J. MOFFAT,[3,4] AND GLORIA KOENIGSBERGER[1]
Received 1993 June 3; accepted 1993 August 24

ABSTRACT

A large accumulation of high signal-to-noise, moderate-resolution optical spectra has led to an unprecedented analysis of the radial velocities of emission and absorption lines in the close binary system V444 Cyg (WN 5 + O6 III–V). Improved orbital elements and masses are $K_{WR} = 332.6 \pm 3.0$ km s^{-1}, $K_O = 108.4 \pm 4.7$ km s^{-1}, $a \sin i = 35.8 \pm 0.4\ R_\odot$, $e = 0.036 \pm 0.009$, $M_{WR} \sin^3 i = 8.8 \pm 0.4\ M_\odot$, $M_O \sin^3 i = 26.3 \pm 1.0\ M_\odot$. With $i = 78\overset{\circ}{.}7 \pm 0\overset{\circ}{.}5$ from previous studies, these yield $a = 38.0 \pm 0.5\ R_\odot$, $M_{WR} = 9.3 \pm 0.5\ M_\odot$, $M_O = 27.9 \pm 1.1\ M_\odot$. Other results include (1) the stable presence of short-period pulsations, $P \simeq 0\overset{d}{.}36$ in the O-C deviations from the W-R orbital curve based on the He II 4686 and 5412 radial velocities; (2) supersynchronous rotation of the O star by a factor ~ 2: $v_e \sin i = 215 \pm 13$ km s^{-1}; (3) sensitivity, especially of the He I 4471, 4922, and 5876 lines, to the presence of a wind-wind collision region in the form of a bow shock around the O star.

Subject headings: binaries: eclipsing — stars: individual (V444 Cygni) — stars: Wolf-Rayet

1. INTRODUCTION

Among the Wolf-Rayet (W-R) stars as "arresting physics laboratories" (van der Hucht 1992), the eclipsing binary system V444 Cyg (HD 193576, WR 139) occupies the distinct place as a sufficiently bright ($m_v = 8\overset{m}{.}27$; see van der Hucht et al. 1981), short-period ($P = 4\overset{d}{.}212$), *eclipsing* binary system. It has been observed frequently and systematically using small and midsize telescopes ever since the discovery of its binary nature in 1939 (Wilson 1939). Before 1992, about 270 articles (Forbes et al. 1992) were devoted to a wide variety of items relating to V444 Cygni, from the origin and evolution of massive binary systems to the detailed investigation of the structure of wind-wind interaction zones. Nevertheless, precise answers to the following questions are still lacking.

1. Does this system have a small but definite nonzero eccentricity?
2. Does the W-R component exhibit oscillations that are stable in time (Marchenko 1988a) or epoch dependent?
3. How do the components of a close binary system rotate in the case of nonconservative mass exchange?
4. Can the global structure of the W-R wind be treated as spherically symmetric in the presence of a hot luminous O companion?
5. Is there evidence in addition to that of previous UV (Koenigsberger & Auer 1985; Shore & Brown 1988) and optical data (He II 4686 line; see Marchenko 1988b) for wind-wind interaction in this system?

In an attempt to answer these questions, we have carried out systematic spectroscopic observations of V444 Cyg at the Observatorie du mont Mégantic (OMM) in 1989–1991 and simultaneous photometry and spectroscopy at San Pedro Martir, México (SPM), and Maidanak (Uzbekistan) Observatories in 1992. Some additional spectroscopic data were obtained at the 3.6 m Canadian-France-Hawaii Telescope (CFHT) in 1987. Note that to obtain robust and reliable orbital parameters, one must accumulate a large number of high signal-to-noise (S/N) spectra in order to reduce the influence of large (up to 15%; see Underhill et al. 1988b) cycle-to-cycle variations.

In the first part of this investigation (this paper), we deal with the data obtained at OMM and CFHT. We will discuss improved radial velocity (RV) orbital parameters; evidence of high-velocity gas around V444 Cyg, from the measurements of the interstellar line (IS) velocities at 5350–5770 Å; stable short-period pulsations of the W-R wind, possibly caused by nonsynchronized W-R rotation; asynchronized axial rotation of the O companion; and variability of the He I $\lambda\lambda$4471.48, 4921.93, and 5875.62 lines, possibly caused by wind-wind interaction.

The second part (Paper II) will be devoted to the investigation of the global W-R wind geometry. For this purpose we shall use the rectified light curve obtained in narrow-band continuum to calculate the true relative variations of line flux and profiles for lines of different ionization and excitation level, from the simultaneous SPM + Maidanak spectroscopy and photometry.

2. OBSERVATIONS AND DATA REDUCTION

The majority of the spectra were obtained in 1989–1991 at the 1.6 m telescope of the OMM with the Cassegrain spectrograph + RCA 512 × 320 pixel CCD in two spectral ranges, 4300–5000 Å and 5300–6000 Å. All these spectra have a 2 pixel resolution ~ 2.7 Å and mean S/N (per pixel, continuum level) ~ 210 at 4800 Å and S/N $\sim$ 250 at 5650 Å. During a four-night run in 1987 August, 22 high-resolution spectra were obtained with the coudé spectrograph + 1872 diode Reticon of the 3.6 m telescope at CFHT in the range 5340–5530 Å, at 0.2 Å 2 pixel resolution and mean S/N $\sim$ 240 per pixel at 5470 Å.

All spectra were processed using standard IRAF facilities,

[1] Instituto de Astronomía, Universidad Nacional Autónoma de México, Apartado Postal 70-264, C.P. 04510, México, D.F., México.
[2] Main Astronomical Observatory of the Ukrainian Academy of Sciences, Goloseevo, 252127 Kiev, Ukraina.
[3] Département de Physique, Université de Montréal, C.P. 6128, Succursale A, Montréal, Québec H3C 3J7, Canada; and Observatorie du mont Mégantic.
[4] Visiting Astronomer, Canada-France-Hawaii Telescope, which is operated by the National Research Council of Canada, the Centre National de la Recherche Scientifique of France, and the University of Hawaii.

with some additional programs added. The journal of observations is given in Table 1, with the following comments: column (1) is the heliocentric Julian date of mid-exposure time; column (4) is the orbital phase in accordance with primary minimum light-curve ephemeris, corrected for the rate of period change (Khaliullin, Khaliullina, & Cherepashchuk 1984); columns (5)–(9) are the heliocentric radial velocities for the emission lines N v $\lambda\lambda$4603, 4945, He II $\lambda\lambda$4686, 5412, and absorption line O III λ5592, respectively; all λ_0 are taken from the tables of Reader & Corliss (1980) when available; other λ_0 for some emission blends are from the Smith & Kuhi (1981) atlas and $\lambda_0 = 4944.56$ for N v is in accordance with Striganov & Sventitskii (1968). There is a $\Delta RV \sim 100$ km s^{-1} difference between the N v λ4603 and N v λ4945 RV curves. We will discuss this fact and related problems of the γ-velocity differences derived from N IV, N v and He II lines in Paper II.

3. RESULTS AND DISCUSSION

3.1. *Radial Velocity Measurements and Improved Orbital Parameters*

Since the discovery of the binary nature of V444 Cyg (Wilson 1939) and further refinement of the orbital elements by Wilson (1940), Keeping (1947), Munch (1950), and Ganesh, Bappu, & Natarajan (1967), only two recent attempts (Underhill et al. 1988a, hereafter UYH; Acker, Prevot, & Prevot 1989) have been made to redetermine the orbital parameters on the basis of spectroscopy with modern detectors. The UYH elements are based on 37 high-S/N, high-quality spectra. Among these, only 16 can be considered as a reliable source for measuring the O star RVs using the O III λ5592 absorption line—the best line for this purpose. The strongly phase-dependent shape of the underlying W-R emissions He II λ5412 and especially He I λ5876 (see our Fig. 7) introduces unpredictable shifts in the O star absorption components, which are reflected in the large uncertainties in the orbital parameters individually derived from these lines (see Table 3 of UYH). An additional problem of the limited sample of available (even high-quality) spectra is a significant cycle-to-cycle variability, frequently reported either in photometry (Cherepashchuk & Khaliullin 1973; Khaliullin & Cherepashchuk 1975) or in spectroscopy (Underhill et al. 1988b), resulting in an increase in the uncertainty of the orbital elements. The method of RV determination by Gaussian profile fitting (Acker et al. 1989) of the broad, asymmetric emissions leads to low accuracy of the derived RVs, $\sigma(RV_{WR}) = \pm 60$ km s^{-1}, and as a consequence, low accuracy of all orbital elements. Our large number of sufficiently high S/N spectra should resolve the above mentioned problems.

In order to investigate the stability of the wavelength zero point (λ_0) of the 1.6 m telescope instrumental system and to compare it with λ_0 at CFHT, we have measured all RVs (centroids or gaussian fitting) of the absorption lines in some 70 spectra of two comparison stars, HR 7752 (A1 V) and HR 6930 (A3 Vn) taken at OMM in 1990–1991 (OMM). In combination with measurements of the IS absorption features $\lambda\lambda$5487.31, 5705.12, in the 1989-1991 OMM and 1987 CFHT spectra of V444 Cyg, this provides us with an upper limit of the instrumental zero-point difference, taking into account some possible slight RV variations of both standards (see Hoffleit & Jashek 1984). For the OMM data there is a difference of $\Delta RV_0 = -11.6 \pm 9.5$ km s^{-1} between λ_0 for 1990 minus 1991. For the 1989–1990 period, the difference is negligible: $\Delta RV_0 = 1.2 \pm 3.5$ km s^{-1}. Between the CFHT and OMM spectra, there is a difference $\Delta RV_0 = -10.6 \pm 5.8$ km s^{-1}, most likely caused by the lower resolution of the OMM spectra, and, as a consequence, poorly resolved blend of the two IS absorptions $\lambda\lambda$5487.31 and 5493.8. This would produce some redshift of the resulting IS λ5487.31 profile in the OMM spectra. In summary, the small (≤ 10 km s^{-1}) systematic but known shifts between the λ_0 during the 1987–1991 period permit us to combine all available RVs and determine reliable orbital elements of V444 Cyg. The expected accuracy of the RV measurements is ~ 16 km s^{-1} (standard deviation) for a single measurement and less for the mean values plotted on Figure 1. This accuracy depends only slightly on the equivalent width of the measured lines (EW $\sim$ 0.01–15 Å), being higher for lower EW. We use the mean σ(RV) value as a reasonable approximation for all measured lines with different EW.

The RVs of the W-R spectral features were measured in two ways:

1) By the "centroid" method of the SPLOT routine in IRAF, using the entire profile for O III λ5592 and only the upper portions of the profiles, i.e., at $(0.5–1.0)I_{max}$ intensity level above the continuum for the symmetric N v lines;

2) By bisecting the lines in the following manner: for each interval above the continuum $(0.05–0.15)I_{max}$, $(0.15–0.30)I_{max}$, $(0.30–0.70)I_{max}$, $(0.70–1.00)I_{max}$ the bisector was computed at intensity increments of $\Delta I = 0.025$ for $I \leq 0.3I_{max}$ and $\Delta I = 0.05$ for $I \geq 0.3I_{max}$ and then averaged.

The radial velocities for the He II emission lines were computed using only the measurements obtained by bisecting the profiles at the intensity levels $(0.15–0.30)I_{max}$ (the upper part is affected

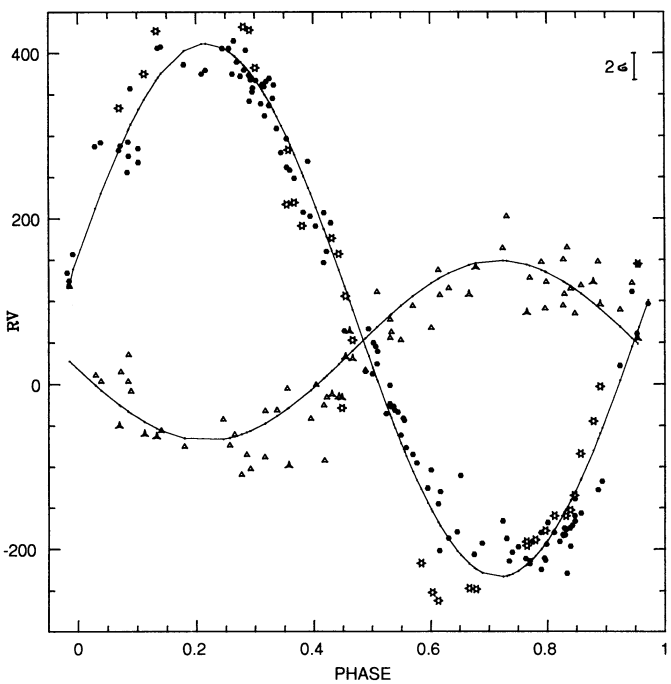

FIG. 1.—V444 Cygni RV orbit. The mean observed RVs for He II $\lambda\lambda$4686, 5412 + N v $\lambda\lambda$4603, 4945 of the W-R component are indicated by filled dots for our data and by open starred points for the data of Underhill et al. (1988a). The O III $\lambda\lambda$5592 RVs of the O component are indicated by open triangles and starred triangles, respectively.

TABLE 1

JOURNAL OF V444 CYG OBSERVATIONS IN 1987–1991

JD (2,440,000+)	OBSERVATORY	EXPOSURE (s)	PHASE[a]	RV (km s^{-1}) N V 4603	N V 4945	He II 4686	He II 5412	O III 5592
7015.785.....	CFHT	1196	0.072	...	...	...	282.5	...
7015.855.....	CFHT	1294	0.088	...	...	...	275.4	...
7015.924.....	CFHT	1500	0.104	...	...	...	284.9	...
7016.063.....	CFHT	1770	0.137	...	...	...	405.9	...
7016.767.....	CFHT	1099	0.304	...	...	...	366.7	...
7016.813.....	CFHT	965	0.315	...	...	...	361.9	...
7016.861.....	CFHT	1019	0.327	...	...	...	336.7	...
7016.946.....	CFHT	1137	0.347	...	...	...	279.7	...
7017.010.....	CFHT	1659	0.362	...	...	...	258.4	...
7017.105.....	CFHT	1857	0.385	...	...	...	207.2	...
7017.764.....	CFHT	1156	0.541	...	...	...	−31.8	...
7017.832.....	CFHT	1148	0.557	...	...	...	−43.9	...
7017.921.....	CFHT	1300	0.578	...	...	...	−95.4	...
7018.000.....	CFHT	1449	0.597	...	...	...	−126.2	...
7018.091.....	CFHT	1747	0.619	...	...	...	−130.4	...
7018.760.....	CFHT	907	0.778	...	...	...	−191.8	...
7018.819.....	CFHT	1140	0.792	...	...	...	−180.2	...
7018.867.....	CFHT	1021	0.803	...	...	...	−168.4	...
7018.913.....	CFHT	897	0.814	...	...	...	−180.3	...
7018.953.....	CFHT	831	0.824	...	...	...	−191.1	...
7018.999.....	CFHT	1192	0.834	...	...	...	−176.3	...
7019.064.....	CFHT	1874	0.850	...	...	...	−139.4	...
7748.579.....	OMM	770	0.028	...	...	...	287.2	10.9
7748.815.....	OMM	600	0.084	...	...	...	292.8	35.6
7756.563.....	OMM	900	0.923	...	...	...	22.0	89.6
7756.819.....	OMM	700	0.984	...	...	...	...	118.1
7758.543.....	OMM	800	0.393	...	...	...	202.7	−41.8
7758.581.....	OMM	600	0.402	...	...	...	190.6	−0.5
7764.579.....	OMM	1182	0.826	...	...	...	−182.5	94.3
7764.589.....	OMM	1515	0.831	...	...	...	−175.0	108.2
7765.610.....	OMM	960	0.073	...	...	...	288.3	15.1
8078.787.....	OMM	1800	0.416	...	...	...	206.7	−92.2
8080.596.....	OMM	950	0.845	...	...	...	−160.1	84.6
8080.641.....	OMM	1000	0.856	...	...	...	−157.2	118.8
8080.762.....	OMM	1500	0.884	...	...	...	−128.2	147.6
8080.792.....	OMM	1000	0.890	−145.2	−272.8	−42.8	...	...
8082.659.....	OMM	700	0.334	...	...	...	308.9	−31.7
8082.732.....	OMM	1200	0.352	...	...	...	261.9	−5.1
8082.787.....	OMM	550	0.365	281.5	114.2	242.7	...	...
8083.638.....	OMM	1200	0.567	...	...	...	−84.8	94.0
8084.595.....	OMM	650	0.794	...	...	...	−213.1	90.6
8084.778.....	OMM	550	0.837	...	...	...	−196.8	114.5
8084.791.....	OMM	320	0.840	−200.2	−288.9	−132.7	...	...
8085.615.....	OMM	1200	0.036	...	...	...	292.1	3.5
8107.629.....	OMM	630	0.262	...	...	...	414.8	−60.6
8107.677.....	OMM	900	0.273	...	...	...	371.8	−109.5
8107.741.....	OMM	900	0.288	...	...	...	341.8	−102.1
8107.761.....	OMM	450	0.294	362.4	241.2	348.5	...	...
8107.822.....	OMM	450	0.308	333.0	229.0	346.4	...	...
8108.594.....	OMM	260	0.491	58.3	−8.6	41.2	...	...
8108.749.....	OMM	650	0.528	...	...	...	−24.0	55.7
8113.570.....	OMM	270	0.673	−225.7	−316.1	−185.4	...	...
8113.627.....	OMM	260	0.686	−206.9	−308.3	−171.2	...	...
8136.592.....	OMM	850	0.138	...	...	...	407.4	−55.9
8137.778.....	OMM	1500	0.419	...	...	...	160.1	−15.7
8138.594.....	OMM	850	0.613	...	...	...	−202.1	107.1
8138.659.....	OMM	720	0.628	...	...	...	−187.0	115.5
8138.721.....	OMM	1000	0.643	−188.7	−299.2	−158.2	...	...
8140.588.....	OMM	630	0.086	...	...	...	357.0	−8.2
8142.745.....	OMM	1500	0.598	...	...	...	−103.9	67.7
8143.542.....	OMM	600	0.788	...	...	...	−224.7	147.1
8143.578.....	OMM	675	0.796	...	...	...	−194.6	122.9
8143.700.....	OMM	675	0.825	...	...	...	−183.8	150.0
8143.713.....	OMM	340	0.828	−187.4	−322.9	−146.1	...	...
8143.749.....	OMM	340	0.837	−186.8	−303.6	−141.4	...	...
8143.784.....	OMM	370	0.845	−187.5	−291.4	−128.2	...	...
8146.567.....	OMM	1200	0.506	...	...	...	24.2	110.9
8146.661.....	OMM	1100	0.528	...	...	...	−1.4	77.5

TABLE 1—*Continued*

JD (2,440,000+)	Observatory	Exposure (s)	Phase[a]	RV (km s^{-1}) N v 4603	N v 4945	He ii 4686	He ii 5412	O iii 5592
8146.686.....	OMM	530	0.534	−31.8	−132.7	−24.1	...	...
8146.718.....	OMM	500	0.541	−37.1	−130.9	−41.4	...	...
8146.777.....	OMM	1200	0.555	−93.8	−185.5	−57.8	...	...
8223.600.....	OMM	600	0.792	...	−330.7	−198.6	...	...
8226.578.....	OMM	1000	0.499	63.6	−42.9	21.4	...	...
8226.595.....	OMM	800	0.503	52.6	−38.3	13.9	...	...
8226.608.....	OMM	800	0.506	48.7	−52.8	14.4	...	...
8228.610.....	OMM	1800	0.982	104.8	−15.7	177.2	...	...
8228.637.....	OMM	2000	0.988	121.1	30.4	211.0	...	...
8430.173.....	OMM	900	0.830	...	...	...	−229.1	164.9
8430.639.....	OMM	380	0.940	...	...	...	111.1	121.8
8430.676.....	OMM	300	0.949	24.7	−99.2	148.4	...	...
8431.753.....	OMM	150	0.205	372.2	260.1	384.5	...	...
8431.782.....	OMM	200	0.212	372.2	277.6	380.3	...	...
8432.629.....	OMM	440	0.413	...	...	...	146.2	−25.4
8432.680.....	OMM	200	0.425	193.0	101.2	182.3	...	...
8437.667.....	OMM	650	0.609	...	...	...	−145.6	137.3
8437.830.....	OMM	371	0.648	−102.3	−226.6	...	...	...
8439.649.....	OMM	537	0.080	...	...	...	256.1	3.6
8439.728.....	OMM	258	0.099	279.5	154.9	262.1	...	...
8440.632.....	OMM	355	0.313	...	...	...	324.1	−32.4
8440.690.....	OMM	135	0.327	358.6	231.6	338.1	...	...
8440.788.....	OMM	210	0.350	279.6	184.1	318.6	...	...
8457.791.....	OMM	550	0.386	265.2	167.3	267.6	...	...
8461.560.....	OMM	430	0.281	...	...	...	403.3	−85.2
8461.690.....	OMM	400	0.312	...	...	...	359.2	−88.0
8461.704.....	OMM	320	0.315	378.2	253.1	357.0	...	...
8461.729.....	OMM	350	0.321	370.4	276.8	353.1	...	...
8461.760.....	OMM	350	0.329	360.6	262.2	353.2	...	...
8462.602.....	OMM	960	0.528	...	...	...	−27.8	62.5
8462.672.....	OMM	750	0.545	...	...	...	−61.7	52.8
8462.690.....	OMM	550	0.549	−36.9	−133.9	−61.4	...	...
8463.604.....	OMM	226	0.766	...	...	...	−217.5	128.2
8465.604.....	OMM	925	0.241	...	...	...	405.5	−42.3
8465.650.....	OMM	950	0.252	...	...	...	405.5	−73.5
8465.674.....	OMM	900	0.258	392.1	239.3	385.1	...	...
8465.706.....	OMM	800	0.265	384.3	289.6	386.1	...	...
8465.759.....	OMM	1000	0.278	362.7	274.4	394.5	...	...
8465.795.....	OMM	750	0.286	348.3	273.7	389.9	...	...
8465.808.....	OMM	850	0.290	349.6	264.0	382.1	...	...
8465.821.....	OMM	900	0.293	334.6	256.7	374.6	...	...
8466.628.....	OMM	550	0.484	...	...	...	15.2	16.9
8466.681.....	OMM	1000	0.497	32.4	−82.3	−20.7	...	...
8466.778.....	OMM	545	0.520	−49.8	−116.4	−49.0	...	...
8467.622.....	OMM	435	0.720	...	...	...	−166.5	164.1
8467.650.....	OMM	490	0.727	...	...	...	−187.2	202.6
8467.667.....	OMM	405	0.731	−216.0	−320.8	...	...	...
8467.690.....	OMM	380	0.736	−234.2	−335.4	−150.4	...	...
8467.732.....	OMM	220	0.746	−220.6	−311.2	−168.2	...	...
8467.786.....	OMM	248	0.759	−227.9	−319.2	−195.6	...	...
8467.816.....	OMM	395	0.766	−211.7	−338.0	−200.7	...	...
8468.599.....	OMM	635	0.952	...	...	...	143.2	70.0
8468.667.....	OMM	780	0.968	80.7	−52.5	154.0	...	...
8468.707.....	OMM	460	0.978	106.7	23.2	165.2	...	...
8470.689.....	OMM	285	0.448	...	...	63.9	...	...
8470.725.....	OMM	430	0.457	...	...	63.8	...	...

[a] Phase zero (time of primary light curve minimum) is taken to occur at JD 2,441,164^d.337 + 4^d.212470E + 1^d.35 × 10$^{-8}E^2$ (Khaliullin et al. 1984).

by O star absorption); these are listed in columns (7) and (8) of Table 1.

We have excluded the He II $\lambda\lambda$4542, 4859 lines and C IV λ5806 blend from the RV analysis because of the heavily distorted profiles of the former (due to the O-star absorption lines), and the complicated structure of the latter (blend of two C IV lines with superposed IS absorptions). All He I lines were also eliminated from the RV analysis, because of the presence of strong phase-dependent emission, arising probably from the bow shock region (see below).

The final orbital fit for the W-R component was based on the average RVs of N V $\lambda\lambda$4603.73, 4944.56 and He II $\lambda\lambda$4685.7, 5411.52. The previous inspection of the phase-dependent profile variations shows that the He II and, especially, N V lines are least affected by the wind-wind collision (direct analogy with another W-R + O binary CX Cep; see Lewis et al. 1993).

Before averaging, the RV curve of each line was compared with that for He II λ5412 as a reference. Consequently, the RVs of N V λ4945 were shifted by +107.3 km s^{-1} to match those of N V λ4603. For the definition of the O star orbit, we used only the O III λ5592 RVs. Computation of the orbital elements was performed by applying Bertiau & Grobben's (1969) algorithm with a fixed period $P_0 = 4^d.212435$ and the eccentricity as a free parameter.

Combination of our and UYH's data for He II λ5412 (exactly the same method of profile bisecting) and O III λ5592 gives the orbital elements listed in Table 2. The entire set of RV data together with the orbital fits are shown in Figure 1. The $\gamma_{O,WR}$ velocities, $K_{O,WR}$ and e values are in fairly good agreement with previously obtained values: γ(O) ranges from −33.6 km s^{-1} (Hγ; see Wilson 1940; the negative gamma velocities of Balmer lines simply reflect the detectable mass-loss rates in upper MS stars) to +58 km s^{-1} (He I λ5876; see UYH); γ(W-R) ranges from +16.2 (He II λ4686; see Ganesh et al. 1967) to +100 km s^{-1} (He II λ5412; see UYH); K_O = 98–216 km s^{-1} (UYH); K_{WR} = 301.5–370 (Keeping 1947; UYH); e = 0.0–0.134 (zero assumed by some authors; see Keeping 1947). It is important to note the significant differences of the γ_{WR} derived from different lines: γ(N IV λ4058) = −41.5 to −40 (Ganesh et al. 1967; Munch 1950; UYH) as opposed to γ(He II λλ4686, 5412 + N V λλ4603, 4619, 4595) ≥ 20 km s^{-1} (all previously mentioned authors). We will leave the discussion of this problem for the forthcoming paper. From the calculated orbital elements we obtain immediately the projected semi-major orbital axis $a \sin i = 35.8 \pm 0.4\ R_\odot$, the masses $M_{WR} \sin^3 i = 8.8 \pm 0.4\ M_\odot$, $M_O \sin^3 i = 26.3 \pm 1.0\ M_\odot$, compared with $M_{WR} \sin^3 i$ = 7.7–17.3 $M_\odot$, $M_O \sin^3 i$ = 21.8–37.5 $M_\odot$ from previous derivations (see Table 4 of UYH for references) and the mass function for the O star $f(M_O) = 14.8 \pm 0.4\ M_\odot$. Adopting the well-established value from polarization, $i = 78^\circ.7 \pm 0^\circ.5$ (Robert et al. 1990), we have $a = 38.0 \pm 0.5\ R_\odot$, $M_{WR} = 9.3 \pm 0.5\ M_\odot$, and $M_O = 27.9 \pm 1.1\ M_\odot$. The expected mass of an O6 V star is 37 $M_\odot$ (Schmidt-Kaler 1982)—slightly more for O6 III. The observed O star mass in V444 Cygni corresponds to O7 V, according to Schmidt-Kaler (1982). There are, however, various indications in favor of a downward revision in mass for the most massive stars (e.g. Groenewegen, Lamers, & Pauldrach 1989; Heydari-Malari, Magain, & Remy 1988, 1989).

3.2. *Interstellar Lines in the Spectrum of V444 Cyg*

V444 Cyg is a probable member of the young open cluster Berkeley 86 (Forbes et al. 1992), which in turn is part of the Cyg OB1 association in a hierarchical substructure of this very dynamically active and "violent" region (Nichols-Bohlin & Fesen 1993). The comprehensive study of the *IUE* spectra of the neighboring OB and W-R stars (St-Louis 1990; Koenigsberger 1990; St-Louis & Smith 1991; Nichols-Bohlin & Fesen 1993) reveals the presence of a multicomponent structure of IS features with evidence for both low-ionization C I–II, Si II, Mg I–II, Fe II, and high-ionization N V, C IV, Si IV, Al III lines. These reveal high-velocity components up to $V_{LSR} = -64$ km s^{-1} in N V of WR 136; −57 and −66 km s^{-1} in a mean of low and highly ionized species, respectively, of WR 137; −45 km s^{-1} in C IV, Si IV and −53 km s^{-1} in three low-ionization lines of WR 135; $V_{LSR} = -45$ km s^{-1} in C IV, S IV of V444 Cyg, taking $V_{LSR} = V_{Hel} + 17.5$ km s^{-1} (St-Louis 1990). Both St-Louis & Smith (1991) and Nichols-Bohlin & Fesen (1993) failed to find components with $V_{LSR} \geq -50$ km s^{-1} in the IS spectrum of V444 Cyg. Such high-velocity IS components might be explained to originate in two ways: (1) in gas associated with each W-R star (e.g., in the faint shell nebula in the case of V444 Cyg; see Lozinskaya & Sitnik 1988); or (2) in a supershell(s) enveloping the Cyg OB1, OB3 associations (Phillips, Welsh, & Bettini 1984; Saken et al. 1992). In the first case we would expect to see a larger expansion velocity, $V \simeq$ 70–150 km s^{-1}, as for a local shell expanding into a larger cavity. In the latter case, $V \simeq$ 15–35 km s^{-1} is expected from a rough estimate of the total luminosity of the OB association stars, surrounded by a common supershell(s) (Lozinskaya & Sitnik 1988; Saken et al. 1992). This simple interpretation is complicated by the presence of high-velocity filaments, knots, and other structural elements in the inhomogeneous shells surrounding the central W-R stars, where the resulting spread in RV would create a continuous velocity spectrum due to projection effects.

Following the example of Herbig's (1975) survey, we have measured all visible IS features in each individual spectrum of V444 Cyg and plotted the mean spectrum in Figure 2 (CFHT data) and Figure 3 (OMM) for the region of 5350–5800 Å. In the region of 4300–5000 Å there are few moderately strong IR absorptions, and some of them are severely blended by stellar emission or absorption lines, e.g., λλ4501.8, 4726, red wing of 4428. The same is true for λλ5780.41, 5797.03 and 5888.95, 5895.92, which are not studied here. The results of the RV measurements are given in Table 3, together with $\sigma_{\lambda;W}$ of the mean values. In the case of λλ5487.31, 5509.7, measured both on CFHT and OMM spectra, the weights CFHT: OMM = 2:1 were used to calculate the means.

Table 3 also shows our attempt to identify IS features in the visual region of V444 Cyg. In the catalogue of IS lines, distributed through the SIMBAD database (Garsia 1989), we find only one reference to the measurement of the H and K Ca II lines with $V_{Hel} = -8.6$ km s^{-1} in V444 Cyg, compared to $V_{LSR} = 17$ km s^{-1} of St-Louis & Smith (1991). We have found some new lines (marked by an asterisk in Table 3), which have IS-like profiles. The best candidate for the λλ5349 and 5513 features is Ca I λλ5349.47 and 5512.98. Unfortunately, the remaining Ca I lines, with about the same (expected) intensity,

TABLE 2

ORBITAL ELEMENTS OF V444 CYG

Object	V_0[a]	K	T_0[b]	T_{01}[c]	T_γ[d]	e
W-R star	89.1 ± 1.8	322.6 ± 3.0	8113.174	8113.744	...	0.036
O Star	40.4	108.4 ± 4.7	±0.006	...	8122.765	±0.009

[a] All velocities are given in km s^{-1}; all times in HJD 2,440,000+.
[b] Time of periastron passage.
[c] Time of radial velocity maximum.
[d] Time of gamma velocity passage.

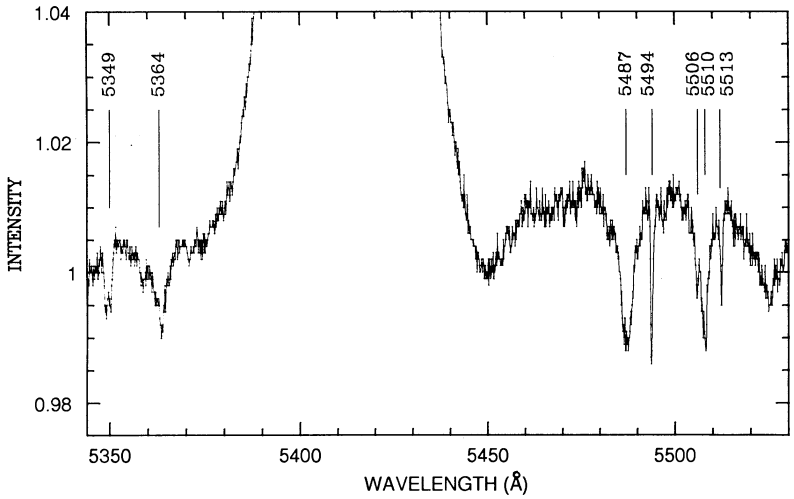

FIG. 2.—Mean interstellar spectrum of V444 Cyg from the CFHT data

are blended with O III λ5592 absorption in the region 5581.97–5601.29 Å (seven lines). The pronounced difference in the $\bar{V}_{\rm Hel}$ of these two features is caused by the two-component structure of λ5349 (see Fig. 2) and the increased uncertainty in the wavelength calibration at the spectrum edge. It is worth noting again that the two-component (or multicomponent) structure was seen by St-Louis (1990) in the C IV λλ1548.19, 1550.76 and the Si IV λλ1393.76, 1402.77 IS lines in the average of 10 spectra of V444 Cyg. The λ5364 absorption might be connected with Fe III λ5363.76 rather than with Fe I λ5364.87. The absence of Fe I λ5371.49, expected to be much stronger than Fe I λ5364.87, argues against Fe I. Among the two possible candidates for λ5506, preference was given to Fe II λ5506.2 rather than Fe I λ5506.69, taking into account (1) the absence of Fe I λ5371.49 and (2) the presence of other Fe II features at λλ5493.83, 5544.76, the latter having some shift due to blending with λ5535. The λλ5545, 5610, 5720 features could be measured only on the mean spectrum, produced from ~50 individual spectra, and are given in Table 3 without σ. The λ5610 feature cannot be identified with any known IS line, so $V_{\rm Hel} = 0$ is assumed for it. Only one possible candidate for λ5720 is Fe III λ5719.88. A more complicated question concerns the identification of λ5747: both N II 5747.30 and Si I 5747.67 are equally good candidates. Some preference for N II 5747.30 was given after the detection of the other component of the N II doublet, N II λ5767.44, only marginally seen in Figure 3, due to blending with the variable wing of C IV λ5806 emission. The blending of N II λ5747.30 with Fe II λ5744.19 (note the asymmetric blue wing) and Si I λ5747.67 would explain the difference in the doublet line strengths.

Following the approach of St-Louis & Smith (1991) and Nichols-Bohlin & Fesen (1993), we can separate the IS lines into three categories: (1) low-velocity gas $|\bar{V}_{\rm Hel}| \leq 25$ km s^{-1}, comprising most of the lines in Table 3; (2) intermediate-velocity gas, $25 \leq |\bar{V}_{\rm Hel}| \leq 50$ km s^{-1} with only one example, Ca I λ5512.98; and (3) high-velocity gas components, $|\bar{V}_{\rm Hel}| \geq 50$ km s^{-1}, for the three lines S II λ5509.7, N II λλ5747.30, 5767.44.

Contrary to what is observed in HD 192163 and other Cyg OB1 stars, V444 Cyg presents only marginal evidence for high-velocity surrounding gas, as found in the UV studies. This reflects either a difference in the spatial structure of the supershell(s) around the OB1, OB3 associations of, what is more probable from our point of view, the relatively thin, weak

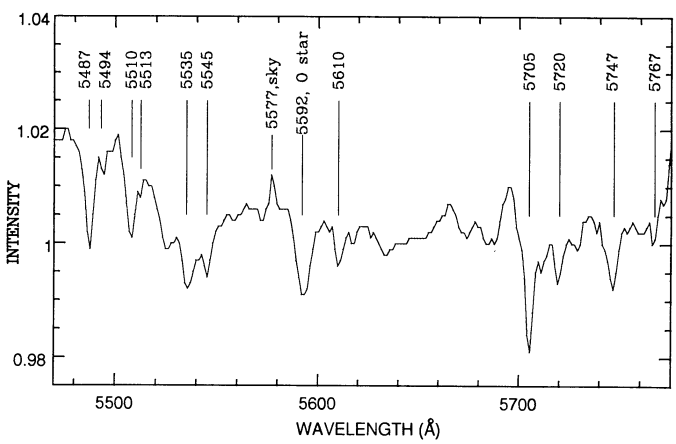

FIG. 3.—Mean interstellar spectrum of V444 Cyg from the OMM data

TABLE 3

INTERSTELLAR FEATURES IN THE RANGE λλ5350–5780 Å

Identification	Observatory	$\overline{V_{\rm Hel}} \pm \sigma_V$ (km s^{-1})	$\overline{W_\lambda} \pm \sigma_W$ (m Å)
Ca I 5349.47*	CFHT	19.0 ± 8.1	16 ± 3
Fe III 5363.76*	CFHT	−10.5 ± 4.8	22 ± 2
IS 5487.31	CFHT + OMM	1.1 ± 3.4	79 ± 4
Fe II 5493.83	CFHT	2.0 ± 0.8	19 ± 1
Fe II 5506.2*	CFHT	−12.8 ± 1.4	9 ± 1
S II 5509.7	CFHT + OMM	−97.0 ± 4.2	48 ± 3
Ca I 5512.98*	CFHT	−33.8 ± 1.3	10 ± 1
IS 5535	OMM	21.1 ± 4.7	64 ± 6
Fe II 5544.76*	OMM	15.1	41
IS(?) 5610.34*	OMM	0.0	32
IS 5705.12	OMM	6.4 ± 2.7	87 ± 4
Fe III 5719.88*	OMM	−15.7	29
N II 5747.30*	OMM	−62.4 ± 6.3	59 ± 5
N II 5767.44*	OMM	−57.4 ± 6.7	31 ± 3

nebula in which V444 Cyg is embedded (actually it was classified as "diffuse nebulosity" by Miller & Chu 1993), in contrast to NGC 6888 around HD 192163.

3.3. *Fast Pulsation of the W-R Wind*

Short-period pulsations ($P_i = 0^d.325$–$0^d.403[\pm 0^d.003]$) were detected for the first time in V444 Cyg by Marchenko & Zhilyaev (1986) in the photometric and spectrophotometric data of several observers. Due to the absence of any such variations in the continuum, it was suggested that the relatively small amplitude periodic change of emission line RVs causes the $\leq 1\%$ flux variations in the narrow-band on-line photometry. Such a modulation is possible if one uses a filter with FWHM comparable to the FWHM of the observed emission lines. This explanation was supported by the discovery of the same periods in the RV data of Munch (1950) (Marchenko 1988a).

The homogeneity of the OMM and CFHT data permits us to carry out a period search on the residual RVs in the 1987–1991 data. Before the analysis, the mean RV curve given in Table 2 was subtracted from the corresponding RVs of He II $\lambda\lambda$4686, 5412, N V $\lambda\lambda$4603+4945 (shifted) and O III λ5592. The residuals were analyzed using a least-squares sine-wave fit (Marchenko & Zhilyaev 1986). This technique was tested many times and provides us with results in good agreement with other standard methods of period search, for example, PDM for the IRAF package. Possible aliases due to nonequidistant time sampling of the data were selected by calculating Deeming's (1975) spectral window. Among the periods with a significance $\geq 99.9\%$ (five in the RVs of He II λ5412 and eight in He II λ4686) only one compatible period appears in both lines: for He II λ5412, $P = 0^d.3586 \pm 0.0001$ ($f = 2.7887 \pm 0.0005$ d^{-1}, full amplitude $A \simeq 50$ km s^{-1}); for He II λ4686 $P = 0^d.3578 \pm 0.0003$ ($f = 2.7950 \pm 0.0026$ d^{-1}, $A \simeq 53$ km s^{-1}, OMM data, 49 points). It is important to note that the data for He II λ5412 includes the Underhill et al. (1988a), CFHT, and OMM measurements, a total of 108 data points. There are no significant periods in the power spectrum of the N V $\lambda\lambda$4603+4945 RV residuals. The same is true for the RV residuals of the O III λ5592 line, in the range $P = 0^d.25$–$1^d.00$, which serves as an additional check for any possible periodicities caused by instrumental effects and data sampling. With respect to any possible signature of nonradial pulsations, we have found two possible periods for the O III line, $f = 4.2961$ and 8.3153 ± 0.006 d^{-1} (fortunately, far beyond the 2.5–3.3 d^{-1} region of our interest). But taking into account that the line profile of O III λ5592 is seriously affected by noise (central depth is 2% below the continuum, i.e., S/N $\sim$ 4–5), the result can be considered as doubtful. The He II $\lambda\lambda$5412 and 4686 data folded in phase with the $P = 0^d.3586$ and $P = 0^d.3578$ periods, respectively, are plotted in Figures 4 and 5.

The period $P \simeq 0^d.358$ lies close to $P = 0^d.364 \pm 0.003$ found for the N V $\lambda\lambda$4603+4619 lines ($A \simeq 32$ km s^{-1}) and $P = 0^d.368 \pm 0.003$ for N IV λ4508 ($A \simeq 40$ km s^{-1}) recovered (Marchenko 1988a) from the Munch (1950) data and close to $P = 0^d.372 \pm 0.003$ and $P = 0^d.371 \pm 0.004$ obtained by Marchenko & Zhilyaev (1986) from the analysis of He II λ4686 variations in narrow-band photometry and estimations of line asymmetry, respectively. One disappointing fact is the absence of short-period pulsations in the OMM N V $\lambda\lambda$4603+4945 data. A periodic signal is also absent in both the 1990 (21 points) and 1991 (28 points) samples separately. A possible explanation is that these N V lines are formed in the dense zone of the rapidly accelerating wind. If the general assumption

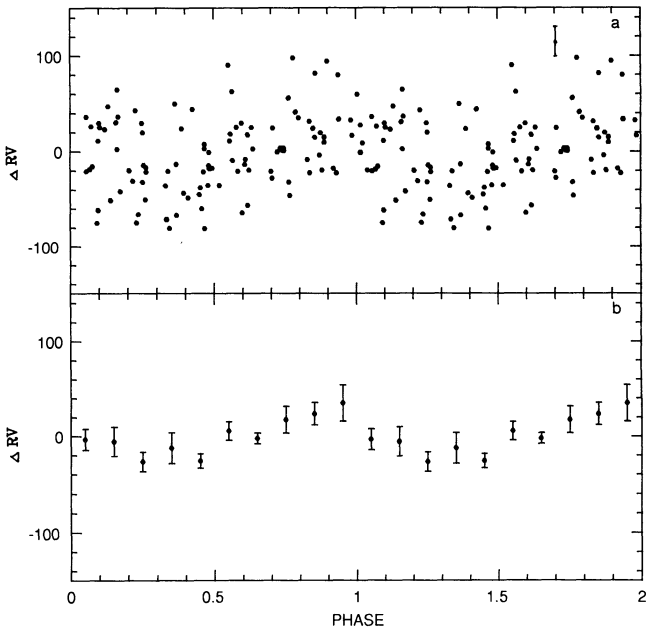

FIG. 4.—Short-period pulsations of the W-R wind: residuals of He II $\lambda\lambda$5412 RVs after subtraction of the mean orbital velocity curve, produced from combining the Underhill et al. (1988a), the CFHT, and the OMM data. Altogether there are 108 points, folded in phase with period $P = 0^d.3586$. (*a*) The total data set; (*b*) the data grouped into $0^p.1$ bins; 2 σ error bars are shown.

$A^2(r) * \rho(r) \sim$ const (in other words, the kinetic energy of the pulsations is conserved) is approximately valid for the $P \simeq 0^d.36$ pulsations, we would expect to see $A \ll 32$ km s^{-1} in N V well below the 99% level of detectability in the OMM N V data. A second explanation for the lack of detectable periodicity in N V may be due to the interference (from the point of view of RV measurements) of short-period pulsations with the orbitally phase-dependent variability of the blue sides of the emission-line profiles.

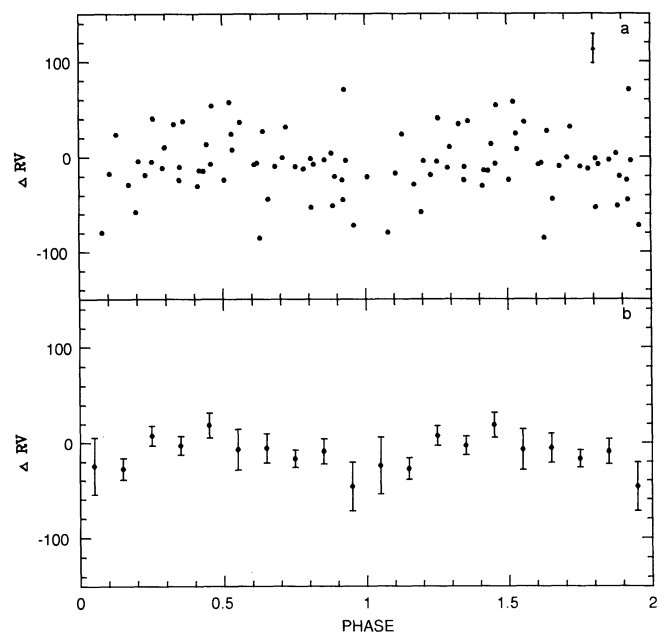

FIG. 5.—Same as Fig. 4, but for He II λ4686 RVs (49 points) and $P = 0^d.3578$. Both sets of data in Figs. 4 and 5 are phased to an arbitarily chosen zero epoch, JD 2,446,620.00 (JD of the beginning of the Underhill et al. 1988a observations).

The presence of $P \sim 0^d.36$–$0^d.37$ variations in emission line RVs during 1949–1991 raises the logical question about its source of stability. Following Osaki's (1986) suggestion, it is possible to generate such pulsations in close binary systems with nonsynchronized orbital/axis rotation by means of "running" tidal waves on the surface of the W-R and O components. However, this is contrary to the arguments that a close companion would circularize the orbit (Tasoul 1990) and synchronized the axial rotation with orbital revolution long before the star leaves the main-sequence (MS) (Zahn 1977). Nevertheless, in the next section we will show that at least in the case of the O star, empirical evidence suggests that corotation does not prevail.

3.4. *Axial Rotation of the O Component*

Prior to the current analysis, only one estimate of the O star projected equatorial velocity $v_e \sin i \sim 220$ km s^{-1} have been made by Underhill et al. (1988b), based on FWHM = 8.3 ± 1.0 Å of O III λ5592. However, this result is presented without any reference to the instrumental profile or other effects which could significantly change the FWHM. An additional problem is that the O III line is a weak absorption feature with central depth only $\simeq$2% below the continuum. Their estimate of its FWHM (two points on the profile) with S/N $\sim$ 4 cannot be very robust and requires confirmation.

We have reevaluated $v_e \sin i$ using the mean absorption profiles of He I $\lambda\lambda$4471, 4542, 4861, and 5412 (OMM and CFHT data separately), following the method of Lewis et al. (1993): each individual spectrum was shifted by the (well-known) orbital velocity of the O component to its gamma-velocity, averaged to produce a mean absorption spectrum with high S/N, and partly smeared out underlying emission features, especially in the case of He II $\lambda\lambda$4542, 4861, and 5412. For comparison, the theoretical profiles for $T = 40{,}000$ K and $g = 4.0$ of He I λ4471, He II 4542, 5412, and Hβ (Auer & Mihalas 1972) were rotationally broadened in accordance with the scheme of Gray (1976) for a rigidly rotating star, taking into account the limb darkening law tabulated by Carbon & Gingerich (1969), which is close to the commonly used $I(\mu, \lambda) = I_0[1 - a(\lambda)(1 - \mu) - b(\lambda)(1 - \mu)^2]$ form (Diaz-Cordoves & Gimenez 1992), but neglecting gravitational darkening (Kopal 1959). The latter would give rise to a maximum difference of $\sim$5% in H_a/H_b (the flux ratio of a two-axis rotating spheroid) in the case of a highly flattened ($r_a/r_b = 1.1$), hot MS star in the range $\lambda\lambda$4500–6000 Å. We do not expect to see such flattening in the case of moderately fast rotating O component. The resulting profile was additionally broadened by a Gaussian instrumental profile with FWHM = 2 pixel = 2.7 Å. The final results of modeling are plotted in Figure 6, where values of $v_e \sin i$ were chosen to match the core of each observed profile best. The discrepancy of the model line wings for He II could arise in four ways: (1) distortion by the underlying emission-line profile; (2) the influence of an additional emission component from the bow shock region (see below), (3) the use of flux profiles (Auer & Mihalas 1972) instead of intensity profiles, which produce slightly shallower and wider lines, $\Delta I \leq 2\%$ for $v_e \sin i \leq 40$ km s^{-1} (Conti & Ebbets 1977); and (4) Stark broadening. The magnitude of the effect due to Stark broadening is related to the value of g used for the calculation of the line profile; i.e., the luminosity class. This uncertainty can introduce differences in the line wings of 20%–40% (Auer & Mihalas 1972). However, the following evidence indicates that the O star companion is a main-sequence star: (1) there is an absorption feature superposed on the He II λ4686 emission line which, if arising in the O star, precludes it from being a supergiant; (2) the mass (27.9 $M_\odot$, this paper) and the O star radius ($R = 8.5\ R_\odot$; see St-Louis et al. 1993) correspond to a V luminosity class (Schmidt-Kaler 1982; Conti & Underhill 1988). The best coincidence of the observed and calculated profiles gives the values of $v_e \sin i$ in Table 4, with $v_e \sin i = 215 \pm 13$ km s^{-1} (formal error of the mean). Adopting $i = 78°.7$, we get $v_e = 219 \pm 13$ km s^{-1}, consistent with the result of UYH. This is almost twice as high as the expected synchronized rotational velocity of the O star with $R_O = 10\ R_\odot$: $v_{synch} = 2\pi R_O/P_{orb} = 120$ km s^{-1}. Unfortunately, the dense wind of the W-R component prevents us from estimating its $v_e \sin i$ from spectroscopy. Nevertheless, the large deviation of v_e from v_{synch} for the O component suggests that a similar situation could prevail for the W-R component, leading to the generation of short-period pulsations by means of a "running" tidal bulge force.

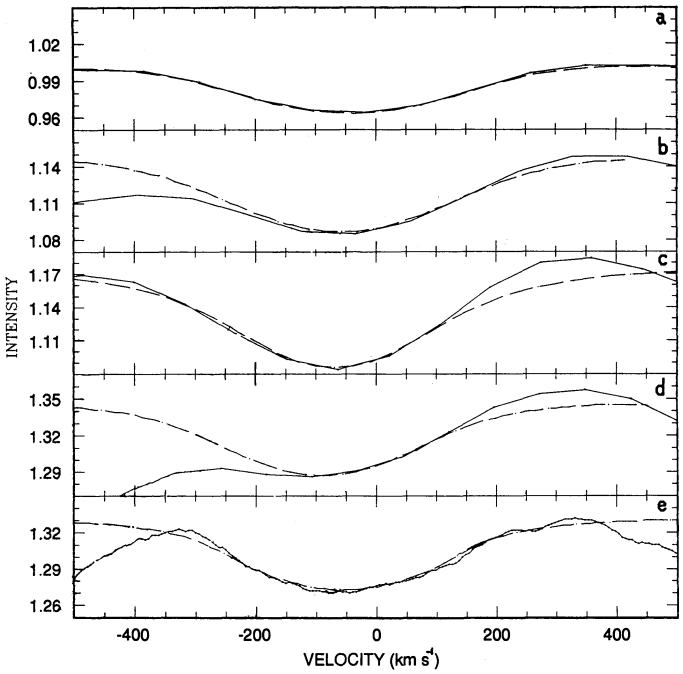

FIG. 6.—Rotation of the O component. The solid lines are the averaged observed profiles after shifting each individual spectrum to the O star gamma velocity. The dashed lines are the model fit mainly to the photospheric absorption line cores with the following $v_e \sin i$ values: (*a*) He I λ4471, 250 km s^{-1}; (*b*) He II λ4542, 225 km s^{-1}; (*c*) Hβ, 175 km s^{-1}; (*d*) He II λ5412 (OMM), 200 km s^{-1}; (*e*) He II λ5412 (CFHT), 225 km s^{-1}.

3.5. *Wind-Wind Interaction from the* He I *Lines*

Since the pioneer theoretical works by Cherepashchuk (1967, 1976) and Prilutskii & Usov (1976) (for the most recent theoretical references, see Stevens 1993), little attention from

TABLE 4

AXIAL ROTATION OF THE O COMPONENT

Line	$v_e \sin i$ (km s^{-1})
He I 4471	250
He II 4542	225
Hβ	175
He II 5412, OMM	200
He II 5412, CFHT	225

the observational point of view has been paid to the problem of wind-wind interaction in W-R + O systems until quite recently. Koenigsberger & Auer (1985) found evidence from *IUE* observations that wind-wind collisions (W-WC) in three out of five W-R + O binary systems studied prevent the O star component's wind from achieving terminal speed in the direction of the W-R star. This could imply that the wind collision occurs very close to the O star. This conclusion was also reached by Luo, McCray, & MacLow (1990), through calculations of the shock structure for the case of V444 Cyg.

Calculations for V444 Cyg by Shore & Brown (1988) led to the prediction for the asymptotic opening angle of the cavity shock region bending back around the O star of 40°. Independent observational evidence for the existence of such a bow shock region (BSH) was found from the analysis of optical spectroscopic and photometric data by Marchenko (1988b), who referred to the BSH as "the additional emission zone." Similar phase-dependent profile variability is seen in CQ Cep (Shore & Corcoran 1992) and CX Cep (Lewis et al. 1993). Stevens (1993) has presented Monte Carlo simulations of the expected profile variability induced by a W-WC, and applied it to V444 Cyg. A systematic search for W-WC effects in UV and optical spectra of O + O systems is being carried out by Gies and collaborators (see Gies, Wiggs, & Bagnuolo 1993). Along different lines, Williams et al. (1990) attributed the periodic formation of dust in WR 140 to the presence of an enhanced W-WC during periastron passage, which leads to sufficient density compression for dust condensation to occur.

The relatively low resolution of the OMM data does not permit one to see detailed BSH-related variations in the He II $\lambda\lambda$4686 and 5412 lines. We will, however, discuss the 1987 CFHT data for He II λ5412, in combination with the moderate-resolution 1992 SPM spectroscopy of He II λ4686 ($\Delta\lambda \sim 0.9$ Å) in the second paper of this investigation. At this point, we will qualitatively describe the easily detected He I line variability in anticipation of a later quantitative approach. Due to the extent

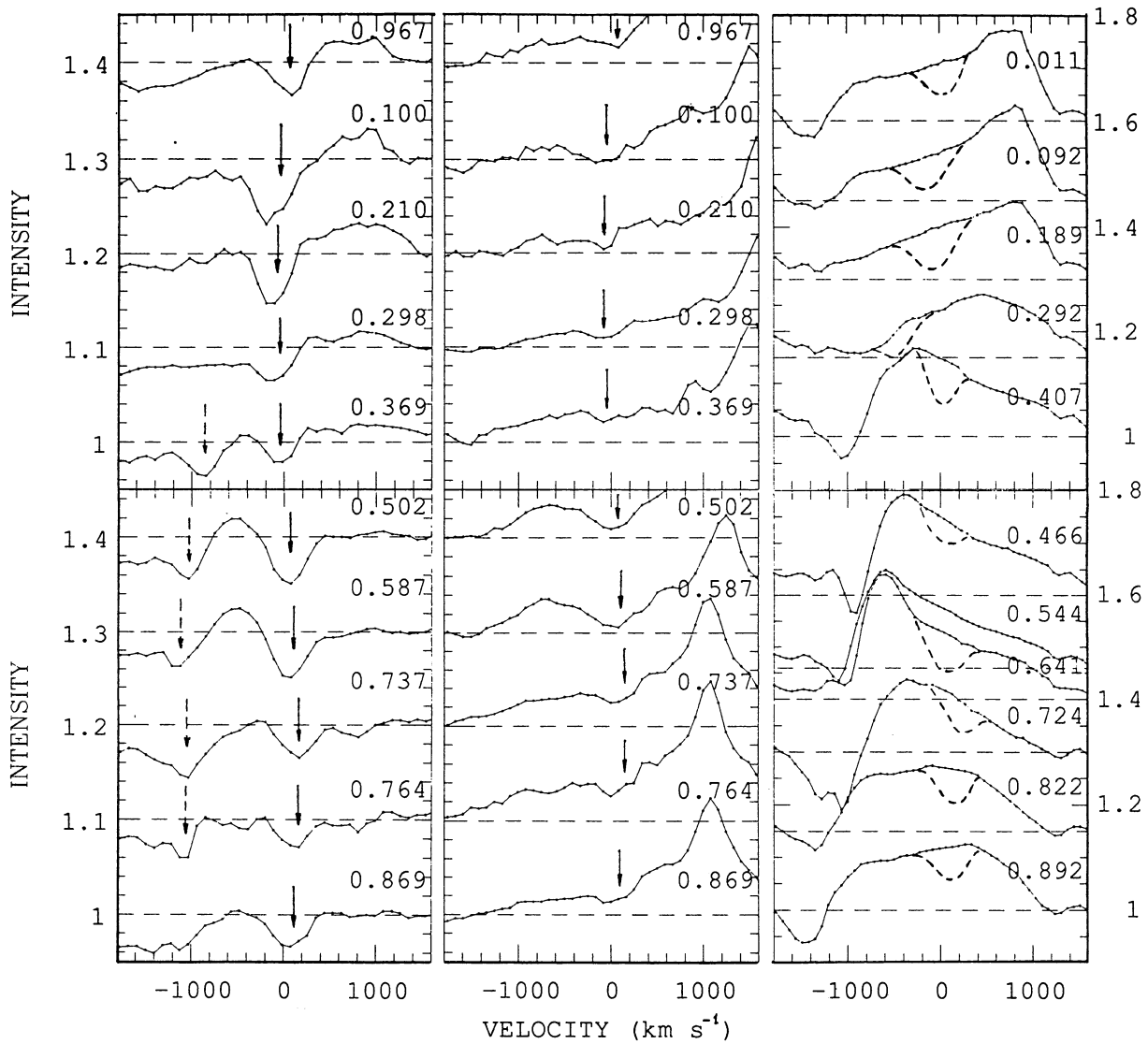

FIG. 7.—Spectra averaged in 0P1 phase bins, of He I λ4471 (*left*), He I λ4922 (*center*) and "reconstructed" He I λ5876 (*right*). The mean phase of each bin is given at the right corner, and the continuum level is marked by a dashed line. Also, the O star absorption in He I $\lambda\lambda$4471, 4922 is indicated by an arrow, and the high-velocity absorption component of He I λ4471 by a dashed arrow. The removed O star absorption in He I λ5876 is shown as a dashed profile.

of the W-R He I formation zone to at least $r \simeq 30R_{WR}$ (as in the similar WN 5 star EZ CMa; see Hillier 1987), the O star orbit lies completely inside it. Thus, the W-WC effects should be seen in the moderate-resolution spectra much more easily in the case of He I than He II (the bulk of the He II emission arises from the region inside the O star orbit and is not so deeply involved in the W-WC process). To demonstrate the W-WC effects on the He I $\lambda\lambda$4471, 4922, and 5876 lines, all available OMM spectra were averaged in 0.1 phase bins: 0P95 to 0P05, 0P05 to 0P15, etc. The mean spectra are plotted in Figure 7. Due to the rapid variation of He I λ5876 at phases 0P45 to 0P55, we divided this subset into 2 bins, ~0P45 to 0P49, ~0P50 to 0P55. Before plotting, the He I λ5876 profiles were "reconstructed" by removing the Na I IS features and O star absorption component. The reconstruction was carried out based on the mean OMM characteristics of Na I [$W_\lambda(5890) \simeq 0.5$ Å, FWHM $\simeq$ 2.8 Å; $W_\lambda(5896) \simeq 0.4$ Å; FWHM $\simeq$ 2.6 Å] and He I photospheric absorption ($W_\lambda \simeq 0.6$ Å, FWHM $\simeq$ 8.2 Å). The removal was performed using the SPLOT task in the IRAF package (linear fit between the edges of the O star absorption). For the sake of simplicity, we did not shift the O absorption He I profiles before averaging, in view of the small RV amplitude of the O star, ± 120 km s^{-1}, and the fact that we do not know a priori the amplitude and eccentricity of the He I RV curves of the W-R component, which may be quite different from the He II and N V orbits.

The behavior of the He I profiles can be consistently explained (see Fig. 8) by the presence of an "additional emission" component which apears redshifted at $\phi \sim 0.9$ to 0.3 (W-R passing in front: here we see matter moving mainly away from the observer in the BSH region around the O star) and blueshifted along with a P Cygni absorption component at $\phi \sim 0.4$ to 0.7 produced when most of the BSH region is pointing toward the observer.

To demonstrate the reality of the small blue/redshifted emission in the He I λ4471, the spectrum-to-spectrum variability of the intensity at the deepest point in the nearby, shallow λ4428 IS feature was evaluated. We find $\sigma(I_{min}) = 0.7\%$, i.e., the maximum expected error of the local continuum level in an individual spectrum is $\pm 1.5\ \sigma(I_{min}) \simeq \pm 1\%$, thus ~3 times less than the intensity of the excess emission.

Because of orbital motion, the BSH presents aberration, with the deviation between its axis of symmetry and the line joining the centers of the W-R and O stars $\Delta\psi \sim \arctan [V_{orb}/V(r)]$, where V_{orb} is the relative orbital motion of the O and W-R components (440 km s^{-1}) and $V(r)$ is the local speed of the W-R wind. To estimate $V(r)$, one can use the velocity law in the form:

$$V(r) = V_\infty \left(1 - \frac{R_*}{r}\right)^\beta ,$$

with $\beta = 1.0$–2.0; $R_* \simeq 3\ R_\odot$ (Cherepashchuk, Eaton, & Khaliullin 1984) or 6 $R_\odot$ (Hamann & Schwarz 1992); $V_\infty = 1785$ km s^{-1} (Prinja et al. 1990), and distance from the W-R star to the BSH formed close to the O star $r \simeq a$ (semimajor axis) $\simeq 38$ $R_\odot$. This gives $V(r) \simeq 1644$–1503 km s^{-1} for $\beta = 1$, and $V(r) \simeq 1514$–1266 km s^{-1} for $\beta = 2$. The latter ($\beta = 2$) is preferable for "early" WN and WC (WNE and WCE) stars (Schmutz et al. 1992), as is the case for V444 Cygni. This leads

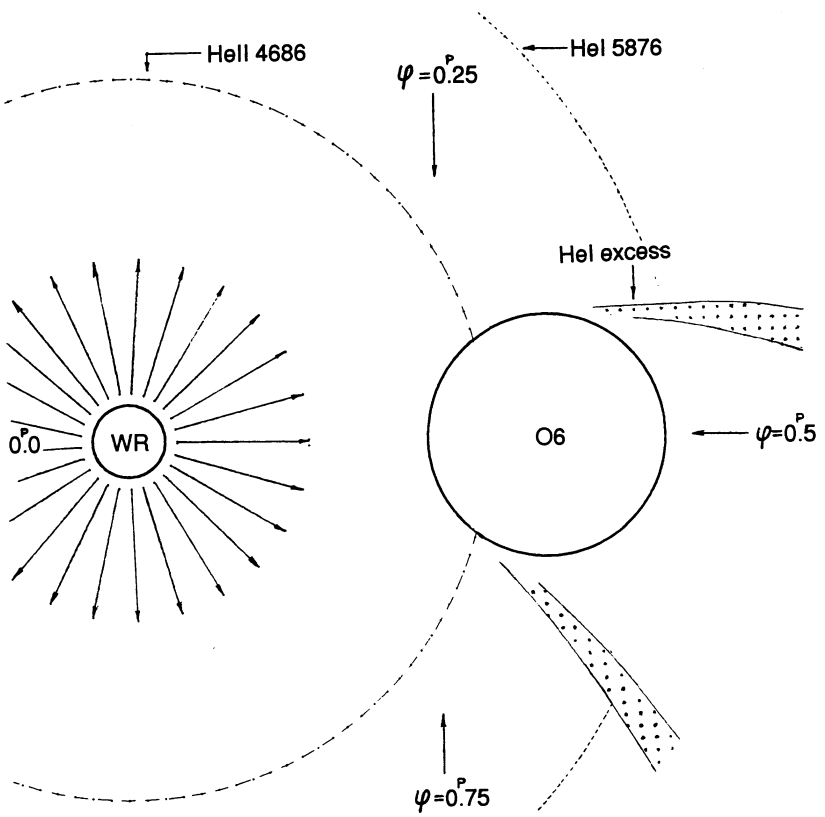

FIG. 8.—Scaled diagram in the orbital plane of the V444 system, showing schematically the ionization structure of the W-R wind (the radii where the emissivity of the He I, II lines reaches its maximum, in accordance with Hillier 1988) and the He I shock cone around the O star.

to a BSH aberration angle $\Delta\psi \sim 16°$–$19°$, i.e., all W-WC phenomena are expected to reveal a phase lag $\sim 0^{p}04$–$0^{p}05$.

It seems remarkable how the narrow blueshifted He I absorption component begins abruptly at $\phi \sim 0^{p}35$ and ends at $\phi \sim 0^{p}8$. This can be explained qualitatively by rapidly cooled gas just outside the trailing BSH arms (see Fig. 8) projected on the stellar disks (both O and W-R in turn; note that the eclipse of the W-R disk by the O star at $\phi \sim 0^{p}5$ is partial). This does not occur between phases $\sim 0^{p}8$ and $\sim 0^{p}35$, when these He I zones are not seen projected on either bright stellar disk. The extent of the He I zones in the BSH arms are guided by the theoretical constraint for cooling times (on the order of hours); see Stevens, Blondin, & Pollock (1992). Note the curvature of the cooled He I zones due to the orbital motion of the O star in the W-R–centered wind. Assuming this absorption to arise in the BSH permits us to put some constraints on the BSH cone angle Θ. According to Stevens et al. (1992) the velocity in the BSH arms where He I is produced would be close to the local unperturbed velocity of the W-R wind. If the velocity of this narrow absorption component $\simeq 1100$ km s^{-1} at the phases around $0^{p}5$ (note the good agreement with Munch's 1950 measurements for the velocity of the blueshifted absorption component of He I $\lambda 4471$) is a line-of-sight component of the velocity into the BSH arm, then taking the reasonable $r \sim a$ distance to this arm, we would obtain $\Theta \sim 82°$–$108°$, larger than $\Theta \sim 40°$–$60°$ given by Shore & Brown (1988). The recent results for the UV, based on a large data set, show that the bow shock is wider than the initial UV data indicated and that the range is closer to that seen in the optical, i.e., the turn-on is at about $0^{p}35$ and turn-off is about 0.65–0.7 (Shore 1993).

We tend to interpret these He I $\lambda 4471$, 5876 $\phi \sim 0^{p}35$–$0^{p}85$ absorption components originating in the densest parts of the BSH arms (see Fig. 8) as due to rapid cooling of the colliding part of the W-R wind (Stevens et al. 1992). The alternate explanation for these narrow absorption components being due to lack of He I in the W-R cavity behind the O star can be excluded. In the case of a cavity, the W-R star profiles would

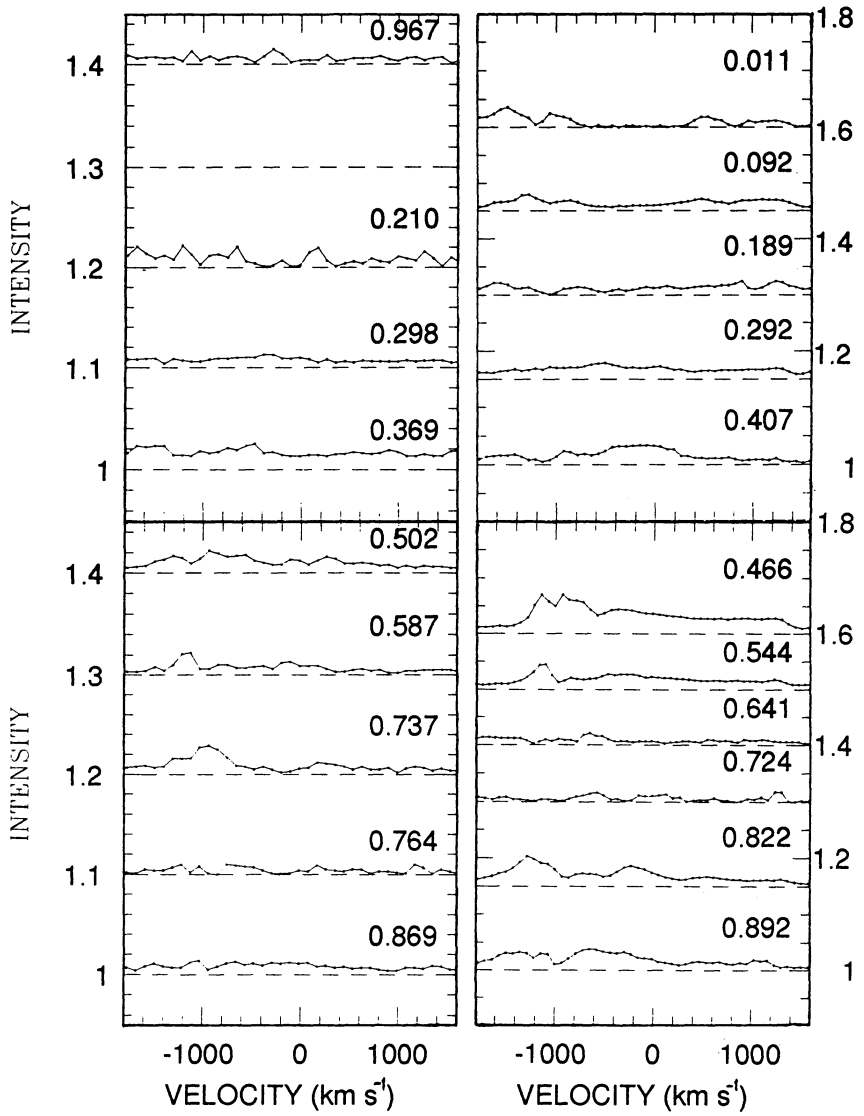

FIG. 9.—Standard deviation of individual spectra in 0.1 phase bins, from the mean spectrum vs. RV from line center, for He I $\lambda 4471$ (*left*) and $\lambda 5876$ (*right*). The mean phases are the same as in Fig. 7.

show absorption or lack of it (depending on the phase) up and *mainly* to V_∞ (Stevens 1993), which is obviously not the case for He I $\lambda\lambda$4471, 5876. For the He I λ5876 line, its "normal" P Cyg absorption component is absent (and partly filled in by resonant scattered He I light) at $\phi \sim 0^p5$–0^p7, due to the absence of part of the W-R wind forming this P Cyg absorption. On the other hand, we do not observe P Cyg absorption from the O star [V_∞(O) $\geq V_\infty$(W-R)] at $\phi \sim 0^p5$–0^p7 and $V(r) \geq V_\infty$(W-R), owing to the weakness of wind-indicating features in the O star He I component in the optical, as opposed to some UV lines formed both by W-R and O star winds. Note the difference between the narrow BSH absorption (He I λ5876, $\phi \simeq 0^p47$) and the "normal" W-R He I λ5876 P Cygni absorption arising starting at $\phi \sim 0^p7$. The difference of the He I λ5876 profiles at phases 0.092 and 0.544 gives a rough estimate of the BSH energies: about 30% of the total emission is formed under the influence of the BSH region!

If we were to interpret the traveling emission on the He I λ5876 profile as a "third light" source, e.g., as resonant backscattering of O star continuum light by the near side of the W-R wind, the Doppler shift would be between $V(r)$ for the incoherent and $2V(r)$ for coherent scattering. The detection of a "traveling" emission velocity V(maximum intensity) ~ -600 to -700 km s^{-1} at $\phi \sim 0^p6$, leads us to reject the case of coherent scattering because $V(r) \geq 800$ km s^{-1} is expected for the He I formation zone (Hillier 1987), so that $V(r)$ due to coherent scattering has to be $2V(r) \geq 1600$ km s^{-1}. If incoherent scattering takes place, which is a more appropriate assumption in W-R winds (ionization processes plus excitation by collisions), then the strength of the "additional" emission component at $\phi \sim 0^p1$ and $\phi \sim 0^p6$ should not be the same due to the angular dependence (Ivanov 1973) of the redistribution function. In actual fact, we observe almost equal emission features at these two phases in He I λ4471 (see Fig. 7). In the case of a redistribution function symmetric to the forward and backward scattering angles of photons by an atom (Stevens 1993), the influence of "third light" on the line profiles is practically indistinguishable from the BSH emission component. However, the presence of a blueshifted absorption component in He I λ4471 at $\phi \sim 0^p6$ remains unexplained from the point of view of the "third light" hypothesis.

Another important fact is the following: if we plot the standard deviations of the individual from the mean spectra in each 0^p1 bin versus velocity, it is seen immediately (see Fig. 9) that the variability is mainly concentrated in the $V(r) \sim -1000$ km s^{-1} regions where BSH absorption is well developed at phases $= 0^p502$, 0.578 and 0.737 of He I λ4471, 0^p466, 0.544 of He I λ5876. Further proof of this statement can be found in Figure 10, where we plotted one night of profiles for He I λ4471, during which the variations of the blueshifted component are most dramatic.

The last intriguing detail is the pronounced difference in the He I λ5876 line profile at the two quadratures, from the point of view of complete absence of absorption at $\phi \sim 0^p25$ and strong absorption at $\phi \sim 0^p75$. The key explanation lies in the phase dependence of the V444 Cyg X-ray flux found by Moffat et al. (1982), which was interpreted as an attenuation by the W-R wind of the W-WC zone near the O star. We would expect to see the highest X-ray flux coming mainly from the zone of the highest compression (i.e., in front of the O star relative to the orbital motion). This would produce higher ionization (Hatchet-McCray effect) of the matter in front of the O star, which would lead to the disappearence of He I λ5876 absorption at $\phi \sim 0^p25$. The most recent *ROSAT* data clearly confirm the attenuation of the W-WC zone both by the O ($\phi \sim 0^p5$) and the W-R components ($\phi \sim 0^p0$) (Corcoran et al. 1993), although the difference between $\phi = 0^p37$ and $\phi = 0^p70$ is not so pronounced and needs further study.

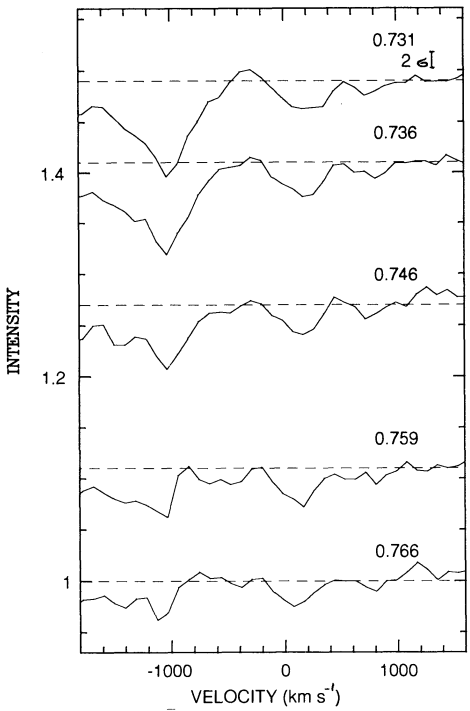

FIG. 10.—JD 2,448,467^{d}667–0.816 sequence of OMM He I λ4471 profiles. Note the significant variations of the blueshifted component. The corresponding phases are given at the right. The separation between the spectra is proportional to the time interval between the subsequent exposures. The continuum is marked by a dashed line.

4. SUMMARY

1. A large number of high S/N spectra of V444 Cyg in the regions 4300–5000 Å and 5300–6000 Å has led to significantly improved orbital parameters: $K_{WR} = 322.6 \pm 3.0$ km s^{-1}, $K_O = 108.4 \pm 4.7$ km s^{-1}, $e = 0.036 \pm 0.009$, which yield the masses, $M_{WR} \sin^3 i = 8.8 \pm 0.4\ M_\odot$, $M_O \sin^3 i = 26.3 \pm 1.0\ M_\odot$.

2. Detailed analysis of the interstellar absorption line velocities in the spectrum of V444 Cyg provides only marginal evidence for the existence for high-velocity gas surrounding V444 Cyg.

3. From the analysis of the O-C deviations in He II $\lambda\lambda$4686, 5412 RVs, we confirm the presence (stable over $\sim$40 yr) of short-period pulsations in the W-R wind, with $P \simeq 0^d36$. The possible energy source of such pulsations could be a tidal force bulge travelling on the surface of the W-R (or O) star. This interpretation relies on desynchronization of axial rotation and orbital revolution.

4. The O component is rotating at $v_e \sin i = 215 \pm 13$ km s^{-1}, twice as fast as the velocity expected from the synchronized axial/orbital rotation.

5. Any modeling of the He I profiles in the spectra of close W-R + O binaries has to account for a bow shock emission component. This may reach up to 30% of the total emission in the He I λ5876 line of V444 Cyg.

This work was carried out under the financial aid of NSERC (Canada), FCAR (Quebec), UNAM/DGAPA 104591, and CONACYT (México). S. V. M. would like to acknowledge Benoit Sanscartier for an introduction to the IRAF package, C. Robert for kind first-stage reduction of the CHFT spectra of V444 Cyg, and A. M. Cherepashchuk for discussions of some aspects of wind-wind collisions in close binary systems. We thank S. Shore for valuable comments and L. Drissen, A. Grandchamps, P. Bartzakos, and N. Drouin for helping obtain the CFHT and some of the OMM spectra.

REFERENCES

Acker, A., Prevot, M.-L., & Prevot, L. 1989, A&A, 226, 137
Auer, L. H., & Mihalas, D. 1972, ApJS, 24, 193
Bertiau, F. C., S.J., & Grobben, J. 1969, Ric. Astron., 8, 1
Carbon, D. F., & Gingerich, O. 1969, in Proc. 3rd Harvard-Smithonian Conf. Stellar Atmospheres, Theory and Observations of Normal Stellar Atmospheres (Cambridge: Cambridge Univ. Press), 401
Cherepashchuk, A. M. 1967, Perem. Zvezdy, 16, 226
———. 1976, Soviet Astron. Lett., 2, 138
Cherepashchuk, A. M., Eaton, J. A., & Khaliullin, Kh.F. 1984, ApJ, 281, 774
Cherepashchuk, A. M., & Khaliullin, Kh.F. 1973, Soviet Astron., 50, 516
Conti, P. S., & Ebbets, D. 1977, ApJ, 213, 438
Conti, P. S., & Underhill, A. B. 1988, O Stars and Wolf-Rayet Stars ed. S. Jordan & R. Thomas (NASA SP-497)
Corcoran, M. F., Shore, S. N., Swank, J. H., Heap, S. R., Rawley, G. L., Pollock, A. M., & Stevens, I. 1993, in Massive Stars: Their Lives in the Interstellar Medium, ed. J. P. Cassinelli & E. B. Churchwell (ASP Conf. Ser., 35), 260
Deeming, T. J. 1975, Ap&SS, 36, 137
Diaz-Cordoves, J., & Gimenez, A. 1992, A&A, 259, 227
Forbes, D., English, D., De Robertis, M. M., & Dawson, P. C. 1992, AJ, 103, 916
Ganesh, K. S., Bappu, M. K. V., & Natarajan, V. 1967, Kodaikanal Obs. Bull., Ser. A, 184, 93
Garsia, B. 1989, The Interstellar Lines Catalogue, SIMBAD database
Gies, D. R., Wiggs, M. S., & Bagnuolo, W. G., Jr. 1993, ApJ, 403, 752
Gray, D. V. 1976, The Observation and Analysis of Stellar Photospheres (New York: Wiley)
Groenewegen, M. A. T., Lamers, H. J. G. L. M., & Pauldrach, A. W. A. 1989, A&A, 221, 78
Hamann, W.-R., & Schwarz, E. 1992, A&A, 261, 523
Herbig, G. H. 1975, ApJ, 196, 129
Heydari-Malari, M., Magain, P., & Remy, M. 1988, A&A, 201, L41
———. 1989, A&A, 222, 41
Hillier, D. J. 1987, ApJS, 63, 965
Hoffleit, D., & Jashek, C. 1984, The Bright Star Catalogue (4th ed.; New Haven: Yale Univ. Observatory)
Ivanov, V. V. 1973, Transfer of Radiation in Spectral Lines, NBS Spec. Publ., No. 385, 33
Keeping, E. S. 1947, Publ. Dom. Astrophys. Obs. Victoria, 7, 349
Khaliullin, Kh. F, & Cherepaschuk, A. M. 1975, Astrofizika, 11, 593
Khaliullin, Kh. F, Khaliullina, A. I., & Cherepaschchuk, A. M. 1984, Soviet Astron. Lett., 10, 250
Koenigsberger, G. 1990, Rev. Mexicana Astron. Af., 20, 85
Koenigsberger, G., & Auer, L. H. 1985, ApJ, 297, 255
Kopal, Z. 1959, Close Binary Systems (London: Chapman & Hall)
Lewis, D., Moffat, A. F. J., Matthews, J. M., Robert, C., & Marchenko, S. V. 1993, ApJ, 405, 312
Lozinskaya, T. A., & Sitnik, T. G. 1988, Soviet Astron. Lett., 14, 100
Luo, D., McCray, R., & MacLow, M.-M. 1990, ApJ, 362, 267
Marchenko, S. V. 1988a, Soviet Astron. Lett., 14, 103
———. 1988b, Kinematics Phys. Celestial Bodies, 4, No. 6, 36
Marchenko, S. V., & Zhilyaev, B. E. 1986, Kinematics Phys. Celestial Bodies, 2, No. 5, 18
Miller, G. J., & Chu, Y.-H. 1993, ApJS, 85, 137
Moffat, A. F. J., Firmani, C., McLean, I. S., & Seggewiss, W. 1982, in Proc. IAU Symp. 99, Wolf-Rayet Stars: Observations, Physics, Evolution, ed. C. W. H. de Loore & A. J. Willis (Dordrecht: Reidel), 577
Munch, G. 1950, ApJ, 112, 266
Nichols-Bohlin, J., & Fesen, R. A. 1993, AJ, 105, 672
Osaki, Y. 1986, PASP, 98, 30
Phillips, A. P., Welsh, B. Y., & Pettini, M. 1984, MNRAS, 206, 55
Prilutskii, O., & Usov, V. 1976, Soviet Astron., 20, 2
Prinja, R. K., Barlow, M. J., & Howarth, J. D. 1990, ApJ, 361, 607
Reader, J., & Corliss, C. H. 1980, Wavelengths, NSRDS–NBS 68, Vol. 1
Robert, C., Moffat, A. F. J., Bastien, P., St-Louis, N., & Drissen, L. 1990, ApJ, 359, 211
Saken, J. M., Shull, M. J., Garmany, C. D., Nichols-Bohlin, J., & Fesen, R. 1992, ApJ, 397, 537
Schmidt-Kaler, Th. 1982, in Numerical Data and Function Relationships in Science and Technology, Vol. 2b, ed. K. Schaiffers & H. H. Voigt (Berlin: Springer), 1
Schmutz, W., Leitherer, C., & Gruenwald, R. 1992, PASP, 104, 1164
Shore, S. N. 1993, private communication
Shore, S. N., & Brown, D. N. 1988, ApJ, 334, 1021
Shore, S. N., & Corcoran, M. F. 1992, in Proc. IAU Symp. 151, Evolutionary Processes in Close Binary Systems, ed. Y. Kondo, R. F. Sistero, & R. S. Polidan (Dordrecht: Kluwer), 359
Smith, L. F., & Kuhi, L. V. 1981, JILA Rep. 117, 1
Stevens, I. R. 1993, ApJ, 404, 281
Stevens, I. R., Blondin, J. M., & Pollock, A. M. T. 1992, ApJ, 386, 265
St-Louis, N. 1990, Ph.D. thesis, Univ. of London
St-Louis, N., Moffat, A. F. J., Lapointe, L., Efimov, Yu. S., Shakhowskoy, N. M., Fox, G. K., & Piirola, V. 1993, ApJ, 410, 342
St-Louis, N., & Smith, L. J. 1991, A&A, 252, 781
Striganov, A. R., & Sventitskii, N. S. 1968, Tables of Spectral Lines of Neutral and Ionized Atoms (New York: IFI/Plenum)
Tassoul, J.-L. 1990, ApJ, 358, 196
Underhill, A. B., Yang, S., & Hill, G. M. 1988a, PASP, 100, 741
———. 1988b, PASP, 100, 1256
van der Hucht, K. A. 1992, A&A Rev., 4, 123
van der Hucht, K. A., Conti, P. S., Lunstrom, I., & Stenholm, B. 1981, Space Sci. Rev., 28, 227
Williams, P. M., van der Hucht, K. A., Pollock, A. M. T., Florkowski, D. R., van der Woerd, H., & Wamsteker, W. M. 1990, MNRAS, 243, 662
Wilson, O. C. 1939, PASP, 51, 55
———. 1940, ApJ, 91, 379
Zahn, J.-P. 1977, A&A, 57, 383